

# Attenuation in suspensions of irregularly shaped sediment particles: A two-parameter equivalent spherical scatterer model

Arjen S. Schaafsma

*Delft Hydraulics, P.O. Box 177, 2600 MH Delft, The Netherlands*

Alex E. Hay

*Department of Oceanography, Dalhousie University, Halifax, Nova Scotia B3H 4J1, Canada*

(Received 31 July 1996; accepted for publication 11 November 1996)

Results are presented from an acoustic attenuation spectroscopy study of suspensions of irregularly shaped sediment particles and of nominally spherical lead-glass beads. The measured spectra cover a wide frequency band of 1–100 MHz. It is shown that the spectra can be brought into close agreement with the rigid movable sphere model using two equivalent sphere size parameters. One parameter is the diameter  $d_G$  of an equal cross-sectional area sphere, and is used to scale the frequency to obtain the nondimensional size/frequency parameter  $ka$ . The other parameter is the diameter  $d_p$  of an equal volume sphere, and is used to scale the particle volume to obtain the particle number density  $N$ . It was observed that for the irregular particles the attenuation for  $ka > 1$  is enhanced with respect to the sphere case. The observed enhancement factors are considerable: up to 1.6 for natural sand particles and 1.8 for the most irregular particles studied (ground quartz). In terms of the two-parameter model the enhancement factor is equal to a shape parameter  $b_0 = (d_G/d_p)^3$  and can indeed be explained as a shape effect. The implications of this result for the acoustic detection of suspended sediments in aqueous environments are discussed. © 1997 Acoustical Society of America. [S0001-4966(97)00909-0]

PACS numbers: 43.30.Pc, 43.30.Ft, 43.30.Gv, 43.35.Yb [JHM]

## LIST OF SYMBOLS

$a$	particle radius
$a_G$	radius of equal cross-sectional area sphere
$a_m$	measured particle radius
$a_p$	radius of equal volume sphere
$a_0$	scaling parameter for measured particle radius
$b_0$	scaling parameter for particle volume
$C_m$	mass concentration of particles
$C_v$	volume concentration of particles
$d$	particle diameter
$d_s$	average sieve diameter
$d_y$	diameter at $y\%$ of cumulative particle size distribution by volume

$G_p$	geometric cross-sectional area of particle
$k$	acoustic wave number
$N$	number density of particles
$V_p$	particle volume
$V_G$	volume of equal cross-sectional area sphere
$x$	$ka$ , nondimensional size/frequency parameter

## Greek

$\alpha$	linear attenuation constant for pressure
$\lambda$	wavelength
$\rho$	density of particle
$\sigma$	standard deviation
$\Sigma$	total attenuation cross section

## INTRODUCTION

There has been considerable interest in the development of acoustic methods for sediment transport measurement during recent years.<sup>1–16</sup> The main attraction of the acoustic approach is that it has the potential of providing vertical profiles of suspended sediment concentration and size remotely, and therefore with negligible flow disturbance at the bed, with high spatial and temporal resolution. The most direct way to obtain these profiles would be from backscattering measurements, as in acoustic current profiling.<sup>17</sup> This is the reason that most of the interest referred to above has been in backscattering systems. However, the interpretation of the backscattered signals is a rather complex inversion problem, which is far from being solved completely.

The measurement of the frequency dependence of the attenuation (or extinction), has also received some

attention.<sup>6,18–21</sup> This method cannot provide profiles, but it has been shown that it can provide accurate local measurements of the concentration and size in the case of spherical particles.<sup>21</sup> The present paper is a further step in the development of this method, by extending the analysis to irregularly shaped sediment particles, following a semi-empirical approach.

Very few measurements have been made of the scattering cross sections of natural sediment particles. In particular, there have been few measurements made of the total scattering cross section of suspended sand. With respect to the backscattering inversion problem, the total scattering cross section appears in an exponential term (the attenuation due to scattering) in the equation for the backscattered signal amplitude. Therefore the estimated concentrations are rather sensitive to errors in this term.

In this paper results are presented from a series of experiments in which the total scattering cross section was measured in a frequency-swept acoustic attenuation spectrometer, operating from 1 to 100 MHz, for natural sand particles and for lead-glass beads. It is noted that some preliminary results have been presented,<sup>22,23</sup> since the experimental data became available.<sup>24</sup>

The relation between the total cross section  $\Sigma$  and the attenuation constant  $\alpha$  is, by definition,

$$\Sigma = \frac{2\alpha}{N}, \quad (1)$$

where  $N$  is the number concentration of particles in suspension. In principle it is possible to determine  $\Sigma$  experimentally by measuring  $\alpha$  for known values of  $N$ . The measured cross sections can then be compared with theoretical calculations, using a suitable estimate of the scatterer radius  $a$  to normalize the acoustic wave number  $k$ . For particles in suspension, it is usually not possible to measure  $N$  directly. Instead the volume concentration  $C_v$  of the particles is determined, often from a gravimetric measurement of the mass concentration in a sample of the suspension and the known bulk density of the particles. Then  $N$  is given by

$$N = \frac{C_v}{V_p}, \quad (2)$$

where  $V_p$  is the particle volume. If the particle volume cannot be measured directly, it is usually estimated from a measurement of the particle diameter. For spherical particles, the exact relation

$$V_p = \frac{4\pi}{3} a^3 \quad (3)$$

can be used. It is clear that a small error in the estimate of  $a$  will lead to a comparatively large error in  $V_p$ , and therefore in  $N$ . For irregular particles the errors in these estimates are likely to be larger, since the above equation can be used in an effective sense only, and supposes that the relevant (equivalent volume) effective size can be measured.

Consider now the problem of sound scattering in a turbulent suspension of irregularly shaped particles. Because the particles have random shapes and adopt random orientations as a function of time due to the turbulent motion, one might expect that the time-averaged behavior of the scattered sound field could be described, to a reasonable first approximation, by assuming a spherical shape for the scatterers and some effective size. The few available measurements of the total scattering and backscattering cross sections of natural sand particles support this assumption.<sup>6,16,18,20,25-27</sup> The choice of effective size for the equivalent sphere for natural sand grains has not yet been examined, however. It is this question which is investigated here.

It is clear from Eqs. (1)–(3) that two effective sizes for the equivalent sphere are involved: one is required to scale the wavelength to obtain  $ka$ , the other to scale the particle volume to obtain  $N$ . To illustrate, the left-hand side of Eq. (1) can be computed theoretically, for any value of the non-dimensional size/frequency parameter  $ka$ . Comparison with the experimentally determined quantity on the right-hand side then requires a suitable choice of effective radius with which to normalize the values of  $k$  at which the measurements of  $\alpha$  were made. The natural choice for this effective

size corresponds, for measurements of the total scattering cross section, to the average geometric cross-sectional area of the particles. The second effective particle size corresponds to an equivalent sphere with the same volume  $V_p$  as the particle, and is required to convert the measured volume concentration of particles to the number concentration  $N$ . One effective size therefore corresponds to the diameter of a circle of area equal to the projected area of the particle, the other to the diameter of an equal volume sphere. These two sizes will not in general be the same. It may therefore be anticipated that there should be two different renormalization scales involved in making comparisons between total scattering cross-section measurements for irregular particles, and theoretical calculations for spherical scatterers.

## I. EXPERIMENTAL METHODS

### A. Laboratory measuring system

The experimental setup used to perform the acoustic attenuation measurements in the frequency range of 1–100 MHz is shown schematically in Fig. 1. The main features can be summarized as follows. The suspension to be measured is contained in a circuit and circulated by means of a slurry pump. Measuring sections are mounted in a vertical perspex cylinder (inner diameter 10 cm). A diffuser at the top of the vertical cylinder homogenizes the particle suspension. Samples of the suspension can be taken by a suction tube, used to obtain reference values for the mass concentration and the particle size distribution. The temperature of the water is regulated to within  $\pm 0.01$  °C. This is necessary because the temperature dependence of the attenuation is large at higher frequencies, about 80 dB/m per °C at 100 MHz.<sup>28</sup>

The attenuation measurements are carried out with six pairs of diametrically opposed broadband acoustic transducers, placed in two measuring sections. Basically, measurements are taken at a single frequency and the frequency is swept to obtain a spectrum. The signal generation and processing are explained briefly, referring to the block diagram in Fig. 1. Of each transducer pair, one transmits and the opposite one receives. The transmitted signal is a single-frequency sine wave burst. The burst duration is relatively short with respect to the acoustic path length in water, in order to avoid reflections and interference effects. Typical burst lengths are 15  $\mu$ s below 20 MHz and 2  $\mu$ s above. The average amplitude of the received burst signal is determined, digitized, and stored. An average over a large number of bursts (typically 1000) is taken to increase the measurement accuracy. The burst repetition rate is 1 kHz. At each frequency an electronic reference signal is measured, stored, and subtracted from the detected acoustic signal. This partly eliminates the drift and the frequency dependence of the electronic system. The center frequencies of the transducer pairs are 2.25, 4.5, 10, 30, 50, and 100 MHz. The transducers are commercially available, broadband, immersion-type transducers (from Panametrics, except the 4.5-MHz transducers). Their bandwidths overlap partially, so that depending upon frequency, measurements can be taken with one or more pairs. The separations between the transducer pairs are

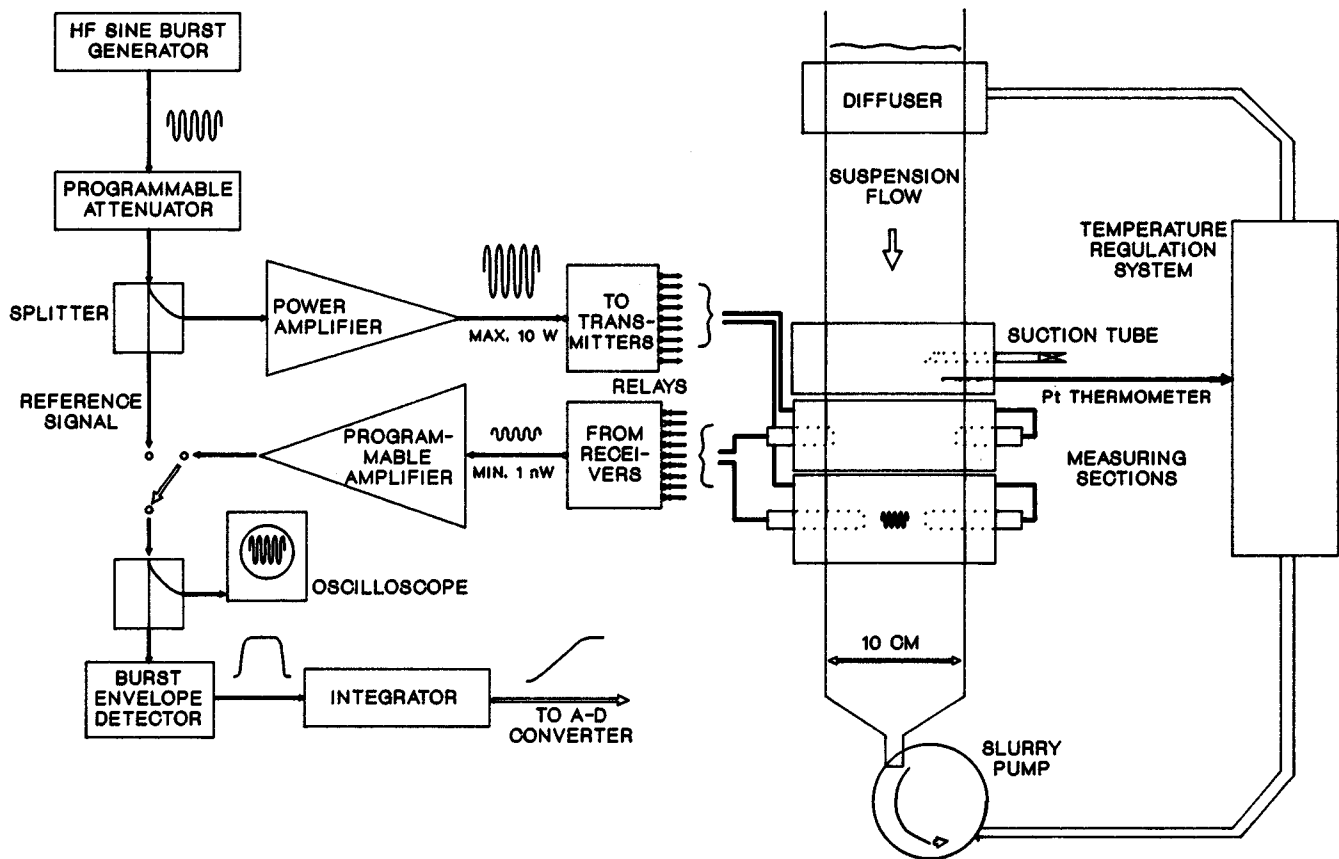


FIG. 1. Sketch of the experimental setup, showing a block diagram of the electronics and the suspension circuit.

given in Table I along with other characteristic properties.

The attenuation spectrum of suspended particles is measured relative to pure water. That is, attenuation data are first collected for pure water, in the above described way, for each transducer pair, at a chosen number of frequencies. These data represent the sum of the electronic and acoustic attenuation, with respect to some fixed reference signal level. Second, a similar set of data is collected for the particle suspension. The difference between the second and the first set of data is the acoustic attenuation spectrum of the suspended particles. Typically, it takes about 1 h to collect a complete data set.

TABLE I. Characteristic parameters of the six transducer pairs used for the attenuation measurements: the center frequency  $f_0$ , the effective transmission bandwidth BW, the diameter of the piezoelectric element  $D_t$ , the near-field distance in water  $r_0$  (at  $f_0$ ), and the transducer separation  $l$ . The near-field distance is defined as the region where the beam is approximately cylindrical [see, e.g., L. E. Kinsler and A. R. Frey, *Fundamentals of Acoustics* (Wiley, New York, 1962), 2nd ed., Chap. 7.12]:  $r_0 = 1.64D_t^2/(4\lambda_0)$ .

$f_0$ (MHz)	BW (MHz)	$D_t$ (mm)	$r_0$ (mm)	$l$ (mm)
2.25	1–3.5	12.7	100	100
4.5	2.4–5.3	5.0	31	100
10	4.9–15	6.35	112	72
30	11.5–34	6.35	336	100
50	12–50	3.18	140	50
100	24–100	3.18	280	28

## B. Validation experiments

The attenuation as defined by Eq. (1) can be measured directly by determining the intensity decay of the acoustic wave in its propagation direction over a known distance. This is straightforward for well-defined wave patterns, like a plane wave or a spherical wave. However, for the present measuring system the transducer configurations are such that most or all of the acoustic path length is within the near-field zone of the transducers (see Table I). It is well-known that in this zone the beam pattern of a transducer has a rather complex structure and is approximately nondiverging. It is expected that, because the transmit and receive transducers used have the same area, an averaging takes place over the structure in the near-field beam pattern. Therefore it is expected that changes in the measured attenuation should represent the average attenuation in the space separating the transducers. Nevertheless, it is worthwhile to verify the influence of near-field effects experimentally. For this purpose, two types of experiments were carried out.

In the first place, the change of the attenuation spectrum of pure water with temperature was measured and compared with results available in the literature. The results of these relative measurements are shown in Fig. 2. The change of the attenuation constant  $\alpha$ , relative to its value at 19.8 °C, was measured for four values of the temperature difference:  $-1.0$ ,  $-0.5$ ,  $+0.5$ , and  $+1.0$  °C. Also shown in the figure are continuous curves, which correspond to the empirical equation given by Fisher and Simmons [Ref. 28, Eq. (10)].

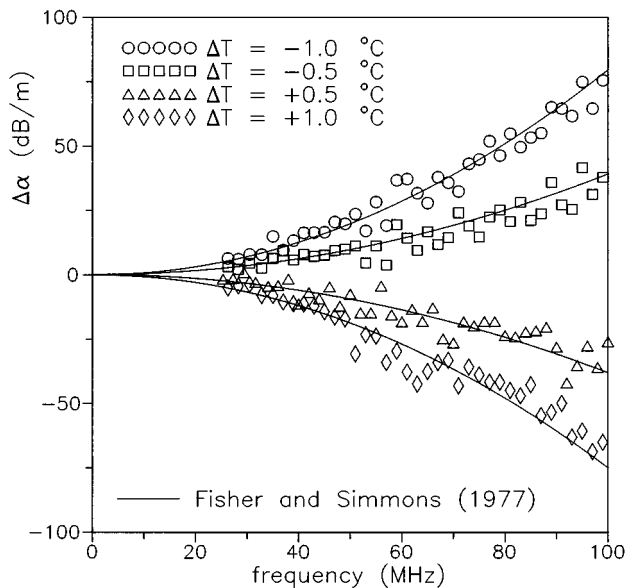


FIG. 2. Measured temperature dependence of the attenuation, relative to its value at 19.8 °C, compared with the empirical equation given by Fisher and Simmons, corresponding to the solid curves (Ref. 28). To improve readability, the data between 1 and 25 MHz, which are close together on the solid curves, are not shown and above 25 MHz only half of the data points are plotted.

This equation agrees to within  $\pm 4\%$  with the experimental data of Pinkerton,<sup>29</sup> which are in the MHz range up to about 70 MHz. Pinkerton verified that his measurements were not affected by near-field effects, by carrying out separate measurements in the near-field as well as in the far-field zones of the transducers. It is shown in Fig. 2 that the present experimental data agree very well with those of Pinkerton. The agreement is within  $\pm 10\%$  (standard deviation) over the whole frequency range.

The second type of experiments involved a detailed comparison between measured and calculated attenuation spectra for spherical lead-glass particles. The result was a good quantitative agreement, the discrepancy was maximum 10% in the high end of the frequency range and smaller in the remaining part.<sup>21</sup>

The above results give confidence that an attenuation

spectrum as measured with the present system, is accurate to within approximately 10% and that effects related to the near-field geometry are not important within this error.

### C. Characterization of suspensions and particles

For a discussion of the acoustic measurements in terms of suspension concentration, particle size, and shape, an independent reference measurement of these parameters is needed. The measurement of the suspension concentration using the suction system of the experimental setup has been developed into a reliable and accurate method. As discussed in some detail before, an accuracy of 5% (standard deviation) has been realized for the mass concentration measurement.<sup>21</sup> In the laboratory experiments suspension concentrations representative for field conditions were used, up to a mass concentration of 5 kg/m<sup>3</sup>, corresponding to a maximum concentration by volume of 0.19%. Because of these low concentrations it is unlikely that multiple-scattering effects are important.

Three sets of particle size fractions were prepared for the present study by sieving or by the use of a hydrocyclone. A reference for the particle size has been obtained by a standard optical diffraction analysis method, using a commercial instrument (Malvern particle sizer 3600 D). Some characteristic results of the particle size analysis for the first set of size fractions, consisting of natural sediment and ground quartz particles, are given in Table II. Average sizes range from about 200  $\mu\text{m}$  down to 30  $\mu\text{m}$ . A second set of size fractions, in approximately the same size range, was made out of nominally spherical lead-glass beads and size analysis results are given in Table III. These particles were chosen for the purpose of comparison with the irregularly shaped sediment particles. Finally, a third set of sediment size fractions was prepared out of three natural sediments of a different origin in two subsets of average size 100 and 200  $\mu\text{m}$ , respectively (see Table IV). In this case also the so-called sphericity was determined, a geological classification by optical microscopy methods.<sup>30</sup>

The densities of the particles are needed to convert measured concentrations by mass to concentrations by volume:  $C_v = C_m / \rho$ . Densities were measured by a volumetric

TABLE II. Summary of optical diffraction (OD) size analysis data and of the two-parameter model interpretation of the acoustic attenuation spectra for the sand sieve size fractions and the quartz hydrocyclone fraction (HC). Assuming a Gaussian size distribution, the standard deviation  $\sigma_m$  was calculated from the OD sizes. The semiempirical analysis was carried out for a single size ( $\sigma_{th}=0$ ) and in four cases also for a Gaussian size distribution, with  $\sigma_{th}$  close to the experimental value. Apart from the indicated exceptions, all measurements were carried out at 19.8 °C.

Particles	Size fraction ( $\mu\text{m}$ )	OD sizes				2-p model			2-p model		
		$d_{16}$	$d_{50}$ ( $\mu\text{m}$ )	$d_{84}$	$\sigma_m$ (%)	$\sigma_{th}$ (%)	$a_0$	$b_0$	$\sigma_{th}$ (%)	$a_0$	$b_0$
Dune sand	180–212	176	212	288	26	0	0.80	1.14	30	0.80	1.18
Assen	90–106	86	110	137	24	0	0.71	1.46	20	0.72	1.48
Assen	45–53	43	60	79	30	0	0.71	1.56	30	0.75	1.61
Assen <sup>a</sup>						0	0.68	1.59			
Assen	45–53	44	62	82	31	0	0.67	1.59			
Assen <sup>b</sup>						0	0.62	1.53			
Quartz	HC4	21	30	45	40	0	0.63	1.82	40	0.60	2.05

<sup>a</sup>Measurement at 9.9 °C.

<sup>b</sup>Measurement at 29.7 °C.

TABLE III. Summary of optical diffraction (OD) size analysis data and of the two-parameter model interpretation of the acoustic attenuation spectra for the sieve size and hydrocyclone (HC) fractions of lead-glass beads. Assuming a (split-)Gaussian size distribution, the standard deviation(s)  $\sigma_m$  was (were) calculated from the OD sizes. The semiempirical analysis was carried out for a single size ( $\sigma_{th}=0$ ) and in most cases also for a (split-)Gaussian size distribution, with a  $\sigma_{th}$  close to the experimental one. Apart from the indicated exceptions, all measurements were carried out at 19.8 °C.

Size fraction ( $\mu\text{m}$ )	OD sizes				2- <i>p</i> model			2- <i>p</i> model		
	$d_{16}$	$d_{50}$ ( $\mu\text{m}$ )	$d_{84}$	$\sigma_m$ (%)	$\sigma_{th}$ (%)	$a_0$	$b_0$ (-)	$\sigma_{th}$ (%)	$a_0$	$b_0$ (-)
180–212	>168	196	<225	<15	0	0.99	1.05	10	0.99	1.07
90–106	85	104	131	22	0	0.94	1.15	20	0.95	1.17
45–53	27	40	50	30	0	0.88	1.44	30	0.90	1.48
45–53 <sup>a</sup>					0	0.88	1.28			
45–53	36	46	60	26	0	0.87	1.24			
45–53 <sup>b</sup>					0	0.85	1.28			
HC4	18	23	43	54	0	0.89	1.40	22/87	0.78	1.59
HC5	12	17	30	53	0	0.95	1.49	29/76	0.71	1.89

<sup>a</sup>Measurement at 11.0 °C.

<sup>b</sup>Measurement at 29.6 °C.

method for the individual size fractions, as a check for homogeneity. For sand and quartz all values were within 1% of the average value of 2650 kg/m<sup>3</sup>. For the lead-glass beads, a value of 2870 kg/m<sup>3</sup> was found for a bulk piece of the same lead-glass and for all size fractions, except for the two smallest sizes (obtained by a hydrocyclone). In the latter cases the densities were 2520 and 2495 kg/m<sup>3</sup>, for the HC4 and HC5 size fractions, respectively (cf. Table III). Possible reasons for this inhomogeneity are discussed below.

A qualitative characterization of particle shape was carried out by scanning electron microscopy (SEM). Typical SEM micrographs for the three sets of size fractions are shown in Figs. 3–5, respectively. The sand particles from the three size fractions obtained by sieving, have an increasingly irregular shape the smaller their average size. This trend is continued for the quartz particles from the hydrocyclone size fraction. One can describe the general shape of these sediment particles as irregular polyhedra, with a varying number of faces and a varying degree of rounding (smoothing) of the edges. In this picture, the 200- $\mu\text{m}$  sand particles are like polyhedra with a relatively large number of faces and relatively rounded edges. On the other, more irregular, end of this scale are the quartz particles (30- $\mu\text{m}$  size fraction), which are closer to polyhedra with a relatively small number

of faces (e.g., a tetrahedron) and further relatively sharp edges.

The lead-glass beads are quite spherical on the whole, but most have surface and volume defects, some particles have a distorted shape. The surface defects are scratches and pits, the volume defects are interior holes, which can be concluded from an examination of the cross sections of the beads, as in a previous study.<sup>21</sup> The number of these defects appears to increase with decreasing average size of the beads, but cannot be quantified accurately. It is noted that a large number of internal cavities could explain the lower measured densities for the two smallest size fractions, mentioned above. These densities are lower with respect to the bulk value by 12% and 13% for the 23- and 17- $\mu\text{m}$  size fractions, respectively. However, an alternative explanation for the lower densities is that these particles have a somewhat different composition: that is, a lower content of lead. It is not unlikely that this can happen in the melt spray production process of the lead-glass beads.

The SEM micrographs for the three 100- $\mu\text{m}$  sand fractions of different origin (Fig. 5) show subtle differences in agreement with the geological sphericity classification (Table IV). In particular, the Assen sand particles appear

TABLE IV. Summary of size and acoustic analysis, as in Table II, for 100- and 200- $\mu\text{m}$  size fractions of some different natural sands. Also given is the result of a geological classification by optical methods, the so-called sphericity, to be compared with the acoustic shape parameter  $b_0$ .

Particles	Size fraction ( $\mu\text{m}$ )	OD sizes				2- <i>p</i> model			Geological sphericity
		$d_{16}$	$d_{50}$ ( $\mu\text{m}$ )	$d_{84}$	$\sigma_m$ (%)	$\sigma_{th}$ (%)	$a_0$	$b_0$ (-)	
Dune sand	180–212	176	212	288	26	0	0.80	1.14	middle
Twente	180–212	171	208	283	27	0	0.79	1.10	high
Ottawa	180–212	178	212	283	25	0	0.81	1.11	middle to high
Assen	90–106	86	110	137	24	0	0.71	1.46	low
Twente	90–106	93	115	142	21	0	0.73	1.32	high
Ottawa	90–106	91	115	143	23	0	0.74	1.28	middle to high

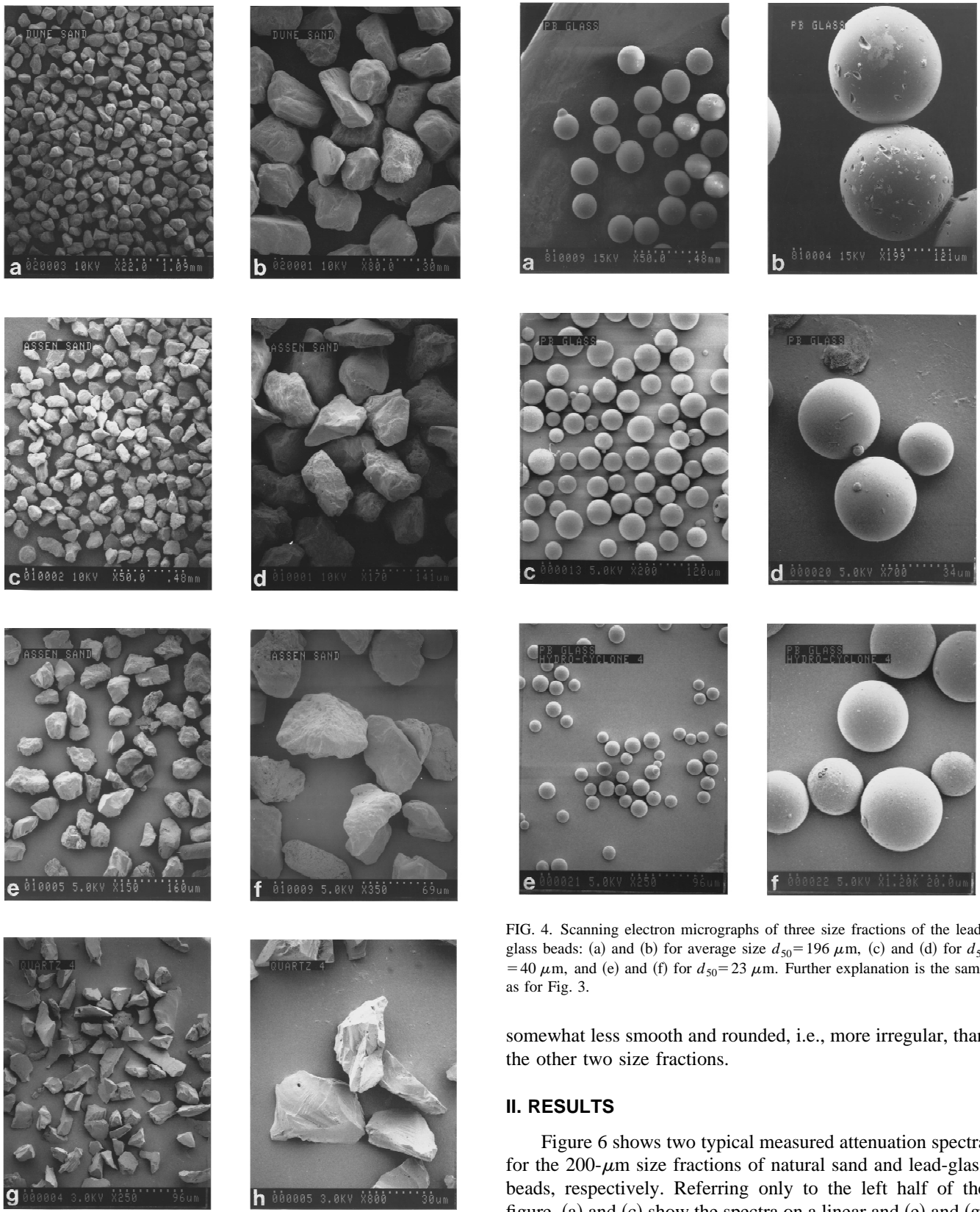


FIG. 3. Scanning electron micrographs of four size fractions of the sand and quartz particles, each at two different magnifications given in the lower right-hand corner of the micrographs together with a size scale. From top to bottom: (a) and (b) dune sand of average size  $d_{50}=212\ \mu\text{m}$ , (c) and (d) Assen sand with  $d_{50}=110\ \mu\text{m}$ , (e) and (f) Assen sand with  $d_{50}=60\ \mu\text{m}$ , and (g) and (h) quartz particles with  $d_{50}=30\ \mu\text{m}$ .

FIG. 4. Scanning electron micrographs of three size fractions of the lead-glass beads: (a) and (b) for average size  $d_{50}=196\ \mu\text{m}$ , (c) and (d) for  $d_{50}=40\ \mu\text{m}$ , and (e) and (f) for  $d_{50}=23\ \mu\text{m}$ . Further explanation is the same as for Fig. 3.

somewhat less smooth and rounded, i.e., more irregular, than the other two size fractions.

## II. RESULTS

Figure 6 shows two typical measured attenuation spectra for the 200- $\mu\text{m}$  size fractions of natural sand and lead-glass beads, respectively. Referring only to the left half of the figure, (a) and (c) show the spectra on a linear and (e) and (g) on a logarithmic  $ka$  scale. The attenuation is presented as  $\alpha/(kb_0C_v)$ , where  $b_0=1$ , a normalization which will be explained below. The wave numbers corresponding to the measurements have been nondimensionalized using the median radii determined by optical diffraction ( $d_m/2$ ), as given in Tables II and III, noting that  $d_m=d_{50}$ . Also shown in the figure is the theoretical attenuation for an acoustically rigid,

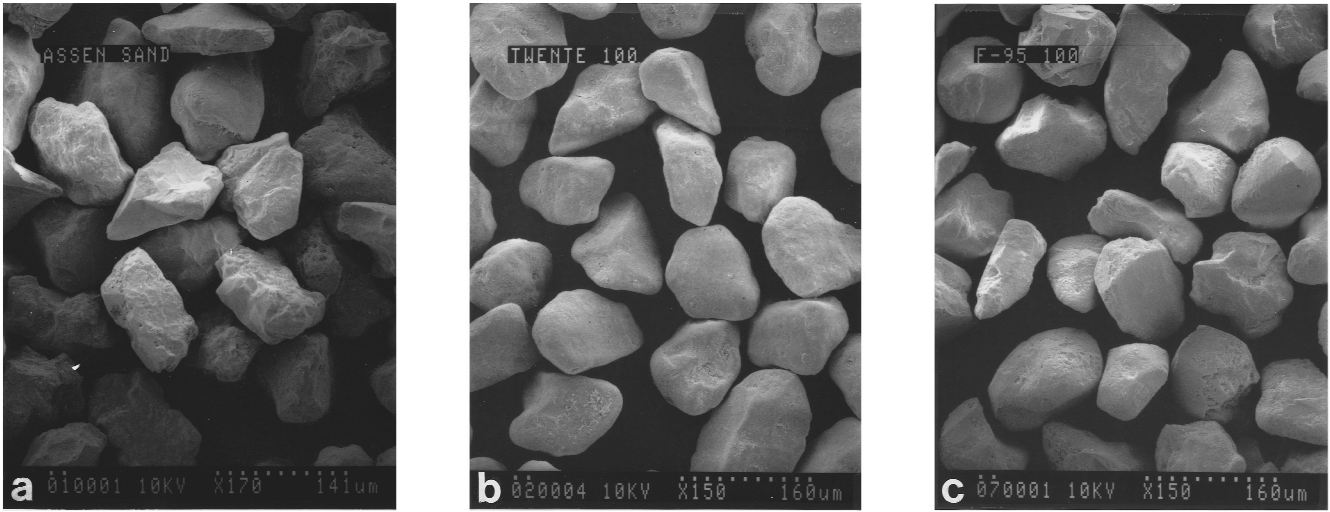


FIG. 5. Scanning electron micrographs of the 90–106- $\mu\text{m}$  sieve size fractions of three sands of different sphericity: (a) Assen, (b) Twente, and (c) Ottawa sand (see Table IV). Further explanation is the same as for Fig. 3.

but mechanically movable sphere with the density of sand, in the same plots as the sand experimental data. Similarly, for lead-glass, the theoretical attenuation for an elastic lead-glass sphere is shown.<sup>21</sup> It can be seen that in the case of the lead-glass beads there is close agreement between the calculated and measured spectra. Also it is seen that for the sand particles the shape of the measured spectrum is very similar to that calculated theoretically, in particular resonance features are absent in the spectra of these nonspherical particles. However, the measured peak attenuation is somewhat greater than predicted by the rigid sphere model and occurs at a somewhat higher value of  $ka$ . It will now be demonstrated that this observed discrepancy in the case of the irregularly shaped sand particles, can be attributed to the scaling problems, related to the choice of effective size, discussed in the Introduction.

Let  $G_p$  be the average geometric (i.e., projected) cross-sectional area of the particles. The logical choice of scale for the total scattering cross section, in the high-frequency limit, is  $2G_p$ . Defining an equivalent circular radius  $a_G$  such that

$$\pi a_G^2 = G_p \quad (4)$$

then Eq. (1) becomes

$$\frac{\Sigma(x)}{2\pi a_G^2} = \frac{V_p}{G_p} \frac{\alpha(x)}{C_v} \quad (5)$$

in which Eq. (2) has been used to eliminate  $N$ , and  $x = ka_G$ . Though the further treatment could have been based on Eq. (5), it has several advantages to remove the explicit size dependence from the right-hand side of this equation, while preserving its nondimensional form, by dividing by  $4ka_G/3$ , yielding

$$\frac{3\Sigma(x)}{8ka_G\pi a_G^2} = \frac{V_p}{V_G} \frac{\alpha(x)}{kC_v} \quad (6)$$

in which now the ratio of the actual particle volume  $V_p$  to the volume of the equal cross-sectional area sphere  $V_G = 4\pi a_G^3/3$  appears on the right-hand side. This ratio is equal to unity for a sphere and this is the main advantage to use

Eq. (6), instead of (5), for an analysis of deviations from the sphere case. Making the substitution  $x = ka_G$ , the above equation can be rewritten as

$$\frac{3\Sigma(ka_G)}{8ka_G\pi a_G^2} = \frac{\alpha(a_0ka_m)}{kb_0C_v} \quad (7)$$

where the nondimensional parameters  $a_0$  and  $b_0$  have been defined such that

$$a_0 = \frac{a_G}{a_m} \quad (8)$$

where  $2a_m$  is the measured particle diameter (here, by optical diffraction) and

$$b_0 = \frac{V_G}{V_p}. \quad (9)$$

It can be seen from Eq. (7) that  $a_0$  and  $b_0$  are scaling parameters,  $a_0$  scaling the measured sizes, and  $b_0$  the measured concentrations. Again, the existence of the two parameters  $a_0$  and  $b_0$  reflects the two scaling problems involved in approximating irregularly shaped particles by spherical scatterers: one being the size required to nondimensionalize the wavelength, the other the size required to determine  $N$  from measurements of  $C_v$ .

Because of the choice of  $a_G$  to scale the acoustic wavelength, so that  $x = ka_G$ , the left-hand side of Eq. (7) is readily computed from the theory for a spherical scatterer. Denoting the left-hand side by  $F_{\text{th}}(x)$ ,

$$F_{\text{th}}(x) = \frac{3\Sigma(x)}{4x2\pi a^2} = \frac{3}{4x^2} \text{Im}[f_{\infty}(x,0)], \quad (10)$$

where  $f_{\infty}(x,0)$  is the forward scattering form factor. Thus it is seen that the choice of the geometric cross section as the appropriate scale for the total scattering cross section leads in a straightforward way to  $a_G$  being the most suitable measure of size with which to nondimensionalize the acoustic wavelength. Note that dividing Eq. (5) by  $x$  leads to a  $1/x^2$  dependence in Eq. (10). As will be seen, this scaling gives the

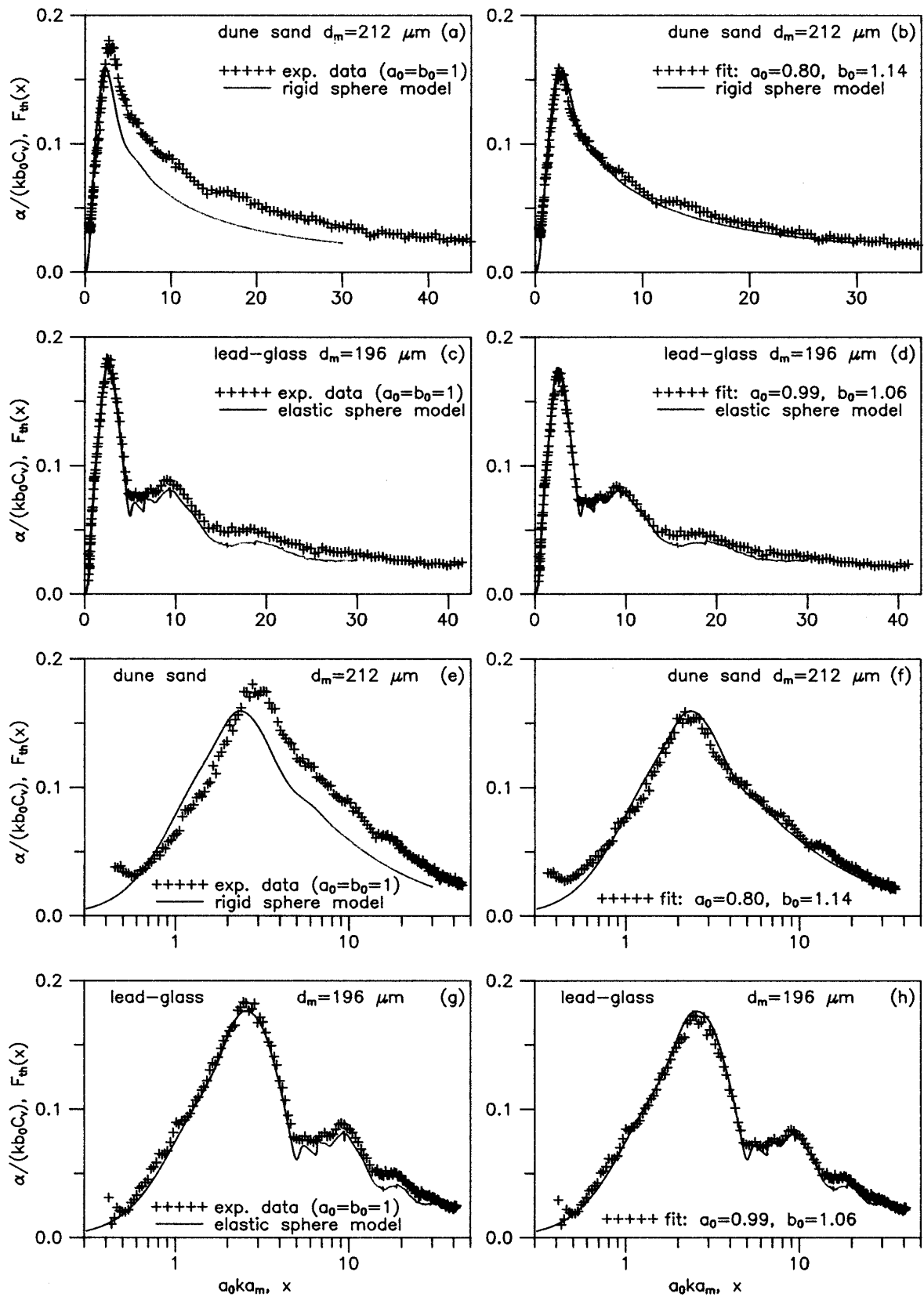


FIG. 6. Comparison of the measured normalized attenuation spectra of the 180–212- $\mu\text{m}$  sieve size fractions of sand and lead-glass beads with the appropriate sphere models (rigid movable quartz and elastic lead-glass, respectively, for which the calculations were made until  $ka = 30$ ). In the left half of the figure the experimental data points are given as they were measured ( $a_0 = b_0 = 1$ ). In the right half of the figure, the measured data have been fitted to the model curves, using a two-parameter fitting procedure. The only difference between the plots (a)–(d) in the upper half of the figure and plots (e)–(h) in the lower half is the normalized frequency scale, which is linear and logarithmic, respectively. Note that there is a significant discrepancy between the as-measured data and the theoretical model for the sand particles, whereas for the lead-glass beads there is a good agreement.

greatest weight to the attenuation measurements in the neighborhood of  $x=2$ , that is where the main broad peak of the spectra is located, which is not unreasonable, since this is the region of the spectrum which provides the size sensitivity. This is seen easily if it is realized that when the normalized spectra are plotted versus frequency  $f$ , the peak position is size dependent (inversely proportional to the size).

The right-hand side of Eq. (7) can be determined from the measurements. That is,

$$F_{\text{exp}}(x) = \frac{\alpha(x=a_0 k a_m)}{k b_0 C_v} \quad (11)$$

for given values of  $a_0$  and  $b_0$ . Here the values of these parameters are the unknowns, and are estimated for each experiment with particles of a given size by least-squares fitting the measurements to the theory for a rigid movable spherical scatterer. This is done by minimizing

$$\chi^2 = \frac{\sum_{j=1}^n (F_{\text{exp},j} - F_{\text{th},j})^2}{(n-2)\sigma^2}, \quad n > 2, \quad (12)$$

where  $\sigma$  is the standard deviation of the measurements,  $n$  is the number of frequencies used in the fit, and  $x_j$  is the value of  $x$  at the  $j$ th frequency. The standard deviation of the measurements  $\sigma$  has been assumed equal for all data points, since the experimental error in the attenuation  $\alpha$  increases approximately linearly with frequency.

The results of applying this procedure to the data in the left half of Fig. 6 are presented in the right half of the same figure. The values of  $a_0$  and  $b_0$  are 0.80 and 1.14 for the 200- $\mu\text{m}$  sand particles. It is important to note that choosing  $a_0$  different from unity results in a rescaling of the values of  $x$  corresponding to the measurements only, and therefore in a displacement of the measured points parallel to the horizontal axis, with the theoretical curve fixed. Similarly, choosing  $b_0$  different from unity amounts to rescaling  $C_v$  only, and results in a vertical displacement of the measured points leaving the theoretical curve unchanged. For comparison, the result of applying the same fitting procedure to the quite spherical lead-glass beads, using the appropriate elastic sphere model in this case, is also shown in Fig. 6 (right half). The values of  $a_0$  and  $b_0$  for the lead-glass beads are 0.99 and 1.06, reflecting the good agreement between spherical scatterer theory and measured data (i.e., within about 5% or better) for these particles.

The result for the 200- $\mu\text{m}$  sand particles in Fig. 6 shows that with the rescaling, the spherical scatterer theory provides an acceptable fit to the data. In Fig. 7 this result is repeated in the two plots at the top and further similar results are shown for the other three size fractions of natural sand and quartz particles listed in Table II. The renormalization works well for all sizes in this range. The quartz particle result is especially interesting because these were the most angular of the particles tested (Fig. 3).

The two-parameter size renormalization also results in a good fit between the rescaled measurements and the theoretical curve for lead-glass beads of different size (Fig. 8; see also Table III) and for natural sand of the same size but different sphericity (Fig. 9; see also Table IV). The results for sands of different sphericity are also interesting. In Fig. 9

it can be seen that the discrepancy between the experimental data and the sphere model is somewhat larger for Assen sand than for Twente and Ottawa sand. This is consistent with a 10% higher value of the parameter  $b_0$  for the scaled measurements. It is noted further that the geological sphericity of the Assen sand is lower than for the other two sands (see Table IV), consistent with the SEM results (see Fig. 5). All values of  $a_0$  and  $b_0$ , corresponding to the results in Figs. 6–9, are listed in Tables II, III, and IV. Summary plots showing the variations of these parameters with particle size and type are presented in Fig. 10.

Before discussing the results further, it is necessary to make two remarks about the spectra and the analysis procedure. In the first place, it is noted that in the low-frequency part ( $ka < 0.5$ ) of most of the spectra, the experimental data have a relatively large uncertainty, because the value of the attenuation is rather low. This is especially the case for the smallest particle sizes. For lead-glass beads there seem to be systematic trends in the low-frequency data, which, although it should be realized that they are overemphasized because of the  $1/f$  weighting, are not understood at present. These data (i.e., the points below  $ka = 0.5$ ) were left out of the fitting procedure.

In the second place it should be noted that in the above analysis, a single size has been assumed for the theoretical curves. However, the actual particle size fractions are distributions which have a nonzero width. The effect this has on the fitted values of the two parameters  $a_0$  and  $b_0$  was assessed as follows. Most of the spectra were also fitted using a theoretical curve, convolved with a Gaussian or split-Gaussian size distribution, as an approximation to the actual size distribution. The width of the distribution was taken close to the experimental one as determined by the optical diffraction size analysis. Results in Tables II and III (last columns) show that the effect on the values of  $a_0$  and  $b_0$  is relatively small if the standard deviation of the size distribution is not larger than about 30%. Two examples are shown in Fig. 11. It is seen that for the 60- $\mu\text{m}$  sand size fraction, the fit and the parameter values are only slightly different from the single size case [see Fig. 7(f)]. The other example of the lead-glass 40- $\mu\text{m}$  size fraction, shows only slightly different parameter values but an improved quality of the fit due to the smoothing of the sphere resonances in the theoretical curve [cf. the single size case in Fig. 8(d)]. For the three cases of the present study where the width of the size distribution is 40% or more, the approximation of the actual size distribution by a Gaussian one is rather crude. The resulting values of  $b_0$  are larger than for the single size case. For the two hydrocyclone lead-glass size fractions, the size distribution is so strongly asymmetrical, that a split Gaussian distribution was used to generate the theoretical curve. In these cases also the resulting values of  $a_0$  are different from the single size fits, they are smaller. The main conclusion for the purpose of the present paper is that the effect of including the particle size distribution in the analysis certainly does not result in smaller values for  $b_0$ . Also it can be concluded that the trend as regards the variation of the two parameters for the different size fractions of sand (and quartz) and lead-glass par-

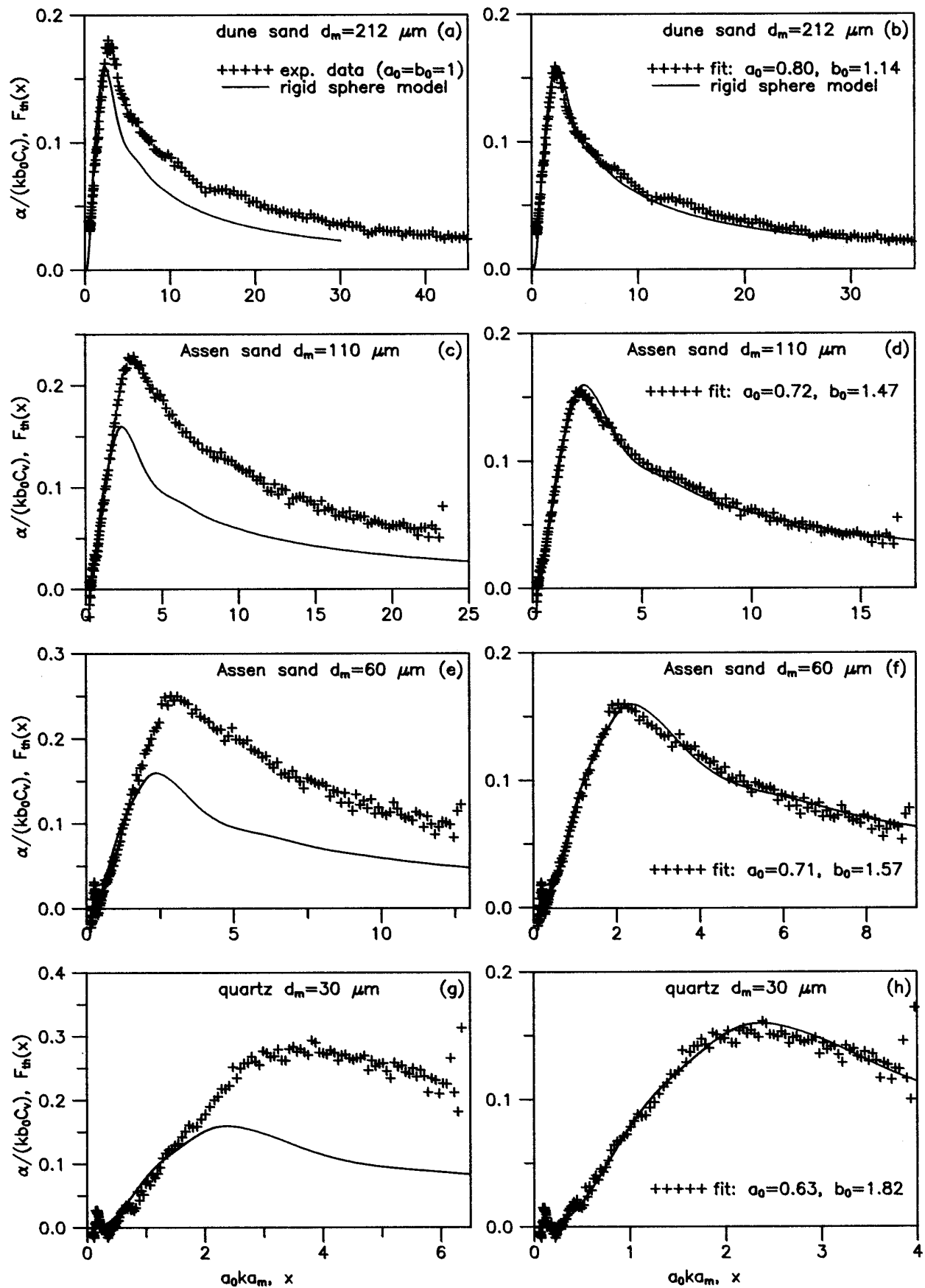


FIG. 7. The left half of the figure shows the measured normalized attenuation spectra of four different size fractions of sand and quartz particles, compared to the rigid movable sphere model for a quartz sphere. The right half of the figure shows the result of scaling the experimental data, using the two-parameter model, to obtain a best fit with the theoretical model.

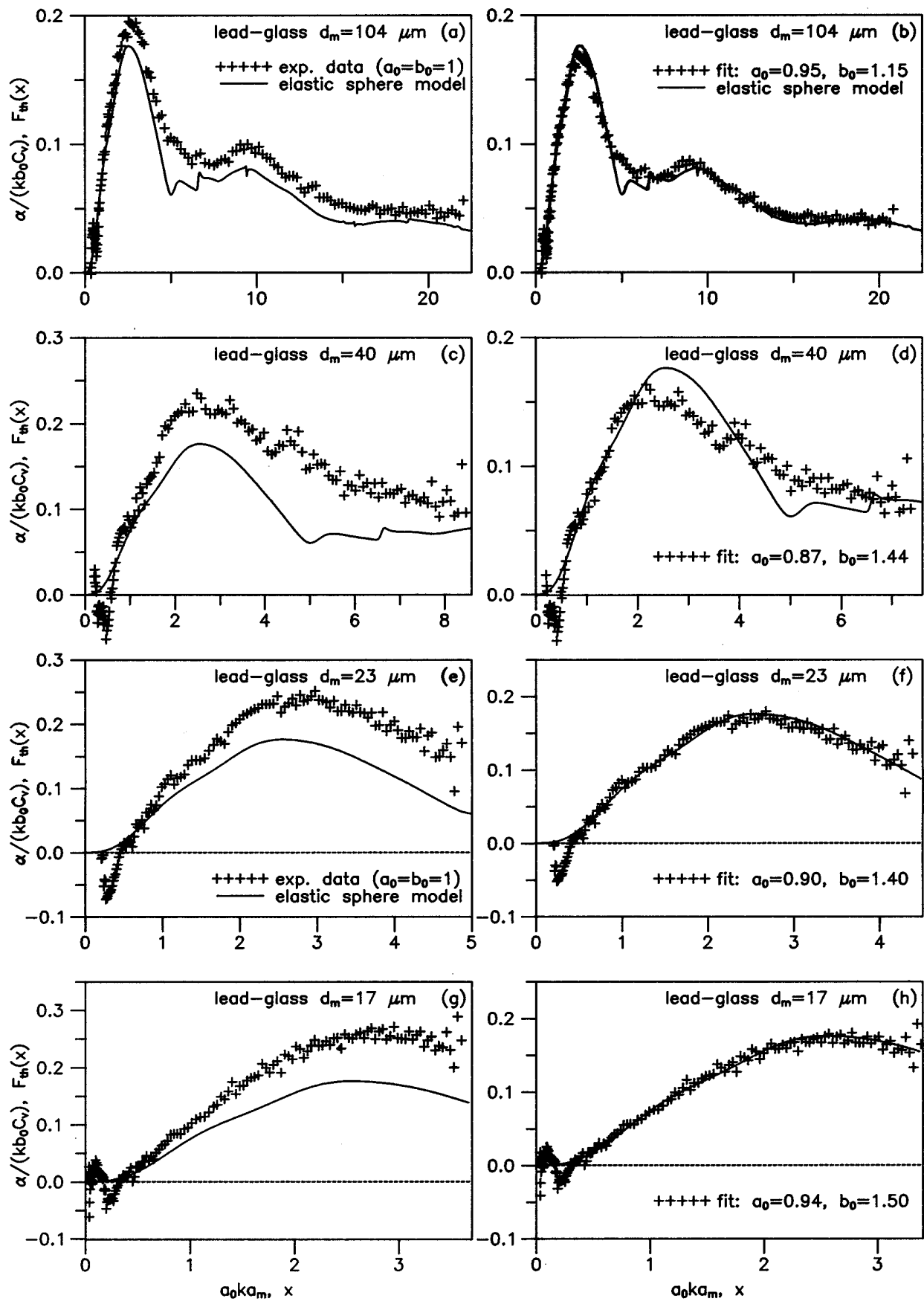


FIG. 8. The left half of the figure shows the measured normalized attenuation spectra of four different size fractions of lead-glass beads, compared to the elastic sphere model for a lead-glass sphere. The right half of the figure shows the result of scaling the experimental data, using the two-parameter model, to obtain a best fit with the theoretical model.

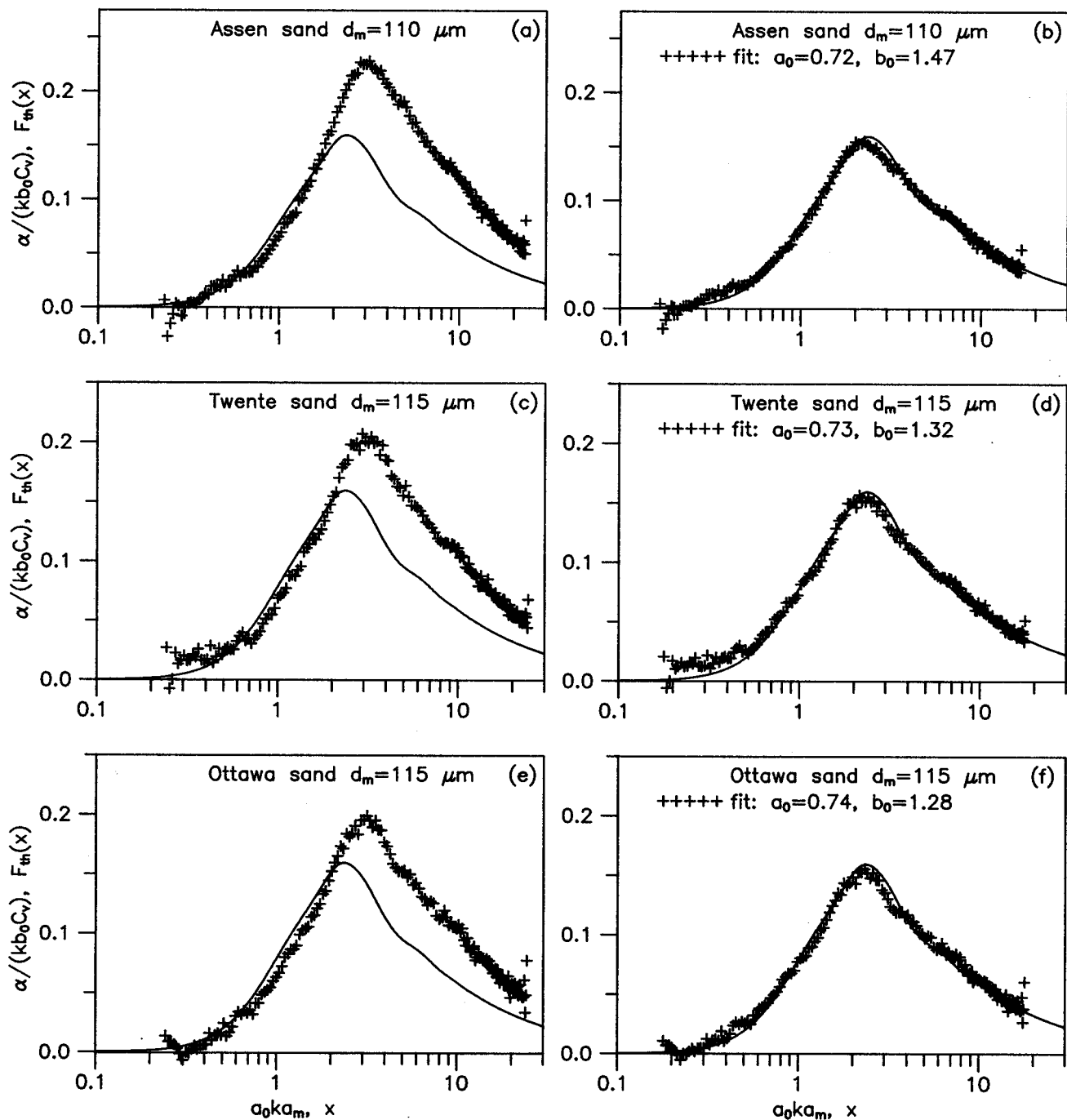


FIG. 9. As-measured, as well as scaled normalized attenuation spectra of 90–106- $\mu\text{m}$  sieve size fractions of three different sands, compared with the rigid movable sphere model for a quartz sphere, are presented in the same way as in the two preceding figures. It is noted that the discrepancy between the experimental data and the sphere model is larger for Aspen sand than for Twente and Ottawa sand and this is reflected in the values of the parameter  $b_0$  for the scaled measurements. This difference correlates well with the geological sphericity of the samples (see Table IV).

icles remains the same, whether or not the size distribution is taken into account.

### III. DISCUSSION

#### A. Physical meaning of $b_0$

The parameter  $b_0$ , as defined by Eq. (9), is determined by the ratio of the two effective volumes  $V_G$  and  $V_p$  so it is seen that  $b_0$  actually is a measure for the departure from a spherical shape, both in terms of (effective) volume and pro-

jected area. The question is then how the relatively large values of the attenuation and thus of the parameter  $b_0$  for the sand and quartz particles (Figs. 7, 9, and 10; Tables II, IV) can be interpreted in terms of what is known about the shape of the particles. Here the results will be discussed in terms of projected area, since this is most directly related to medium- and high-frequency acoustic cross sections, which were the quantities actually measured.

It follows directly from Eq. (9) that  $b_0^{2/3}$  is equal to the ratio of the average projected area of the particle to that of an

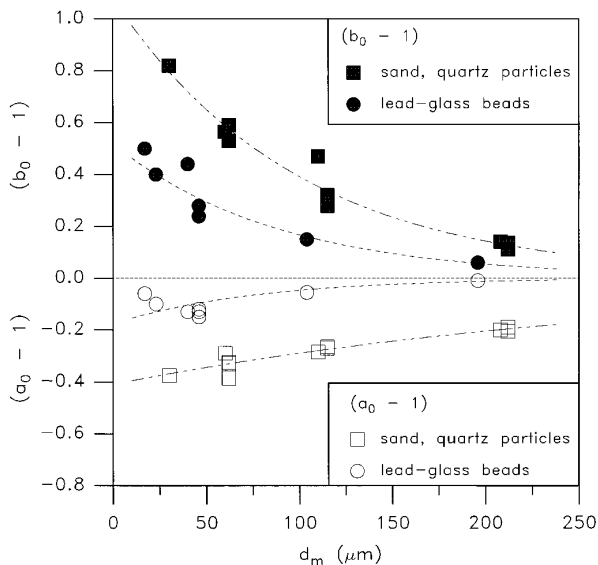


FIG. 10. Summary of all values of the two scaling parameters  $a_0$  and  $b_0$  for the size fractions of sand and quartz particles and lead-glass beads of the present study (see also Tables II, III, and IV).

equal volume sphere. This ratio can be calculated easily for a given convex shape, using a well-known theorem (see, e.g., van der Hulst<sup>31</sup>). The theorem states that the average geometrical cross section of a convex particle with random ori-

entation is one-fourth of its surface area. This provides the possibility to compare the experimental values of  $b_0$  with those for some well-known simple polyhedral shapes, which is done in Fig. 12. The interesting point is that the acoustic shape classification for the natural sand and ground quartz particles, provided by this figure, is consistent with the qualitative shape characterization by scanning electron microscopy as described in Sec. I. Therefore it appears that the observed values of  $b_0$  are consistent with a shape effect.

For the lead-glass beads, the magnitude of the attenuation and so the value of the parameter  $b_0$  is definitely larger than it should be for a perfect sphere, at least for all sizes below  $100 \mu\text{m}$  (Figs. 6, 7, and 10; Table III). The lead-glass beads were chosen to provide an experimental sphere reference for the irregular sediment particles in the same size range. This choice was based on the good agreement between theory and experiment obtained for the 200- and  $100\text{-}\mu\text{m}$  size fractions in a previous study.<sup>21</sup> Therefore the present results for the lead-glass beads are unexpected. However, some suggestions can be made to explain the results. First it is noted that the possibility to explain the lead-glass results as a shape effect, in the same way as the sand and quartz particle results, can be ruled out on the basis of the SEM micrographs (Fig. 4). These show that the majority of the lead-glass beads have a very spherical shape and therefore there will be no increase of the average projected area.

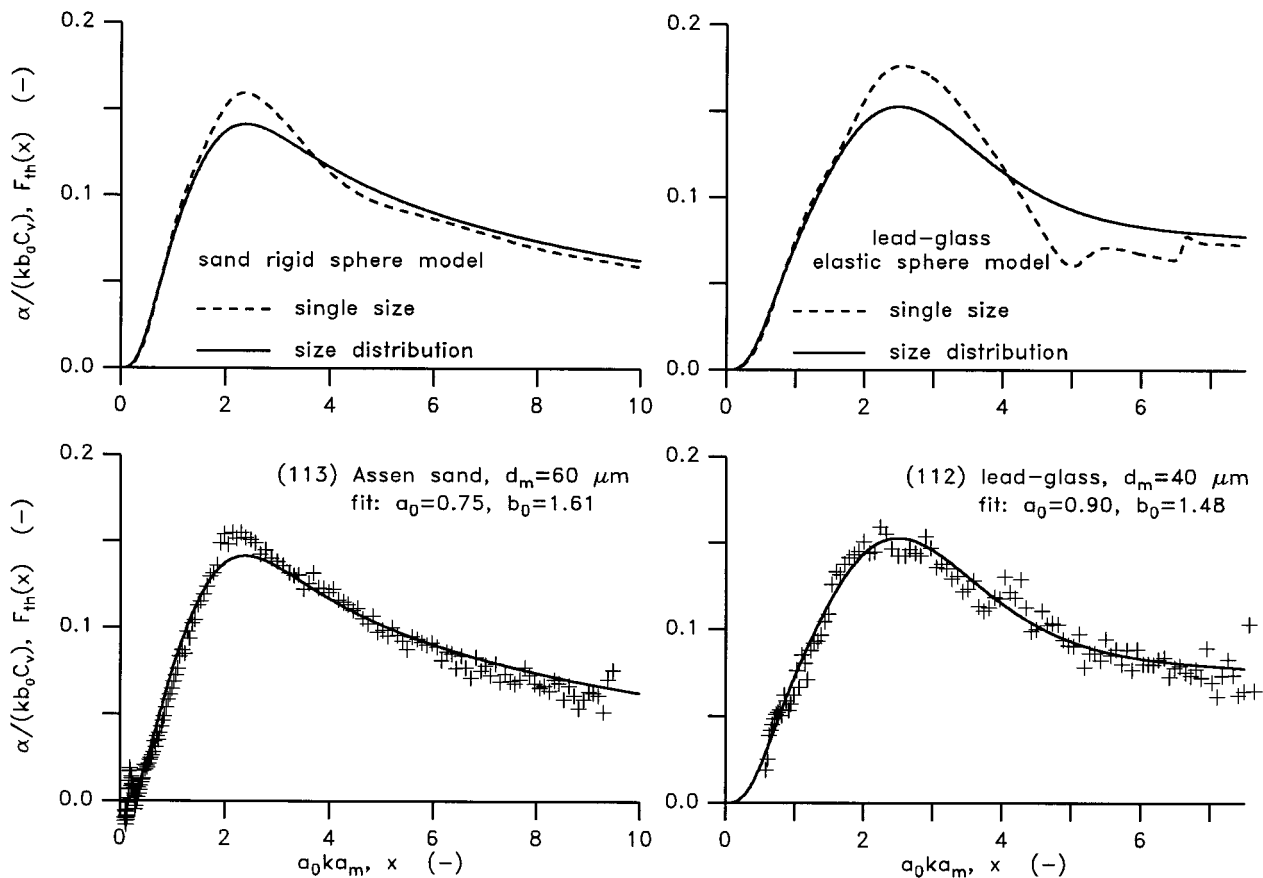


FIG. 11. Example of the effect of taking into account a distribution of sizes, for a Gaussian size distribution with a relative standard deviation of 0.3, which was used to obtain the smoothed (solid) curves for the rigid movable sand or quartz sphere model and the elastic lead-glass sphere model (upper plots). Clearly this also has an effect on the two-parameter scaling procedure (lower plots), where especially the quality of the fit is improved for the case of lead-glass beads (more results are given in Tables II and III).

One suggested explanation is that the extra scattering is due to surface and volume defects (see Sec. I C). However, apart from the observed trend that the number of defects is larger for the smaller size fractions, this contribution cannot be quantified any further without making some assumptions. If it is assumed, for example, that interior holes are responsible for the 12% to 13% lower densities of the smallest lead-glass bead size fractions, this would require a single cavity with a diameter of about half of the diameter of the lead-glass bead. Such cavities would certainly increase the scattering by the beads. Indeed, a strong enhancement of the (backscattering) form function in the  $ka$  range between 2 and 10 was found theoretically for hollow metallic spheres in water by Hickling<sup>32</sup> and the enhancement was found to increase with cavity size.

In the present context, it should also be noted that the extra scattering may have been overestimated by 10%–15% for the two smallest size fractions. The reason is the following. In the analysis given up to this point, the same bulk value of the density has been assumed for all size fractions. This means that the lower measured densities for the two smallest size fractions have been ignored. The lower values of the density may be attributed to the presence of interior holes, or alternatively, to a slightly lower lead content of the beads (ignoring the effect of the holes on the density). Actually, whatever their origin, the lower measured densities should be used in the two-parameter model analysis of the attenuation. This leads to proportionally lower values of  $b_0$  [see Eq. (11)]: 1.23 and 1.29 instead of, respectively, 1.40 and 1.49 given in Table III for the two smallest size fractions. These lower values of  $b_0$  are included in Fig. 12 (only).

## B. The meaning of $a_0$

The parameter  $a_0$ , as defined by Eq. (8), is equal to the ratio of the acoustic cross-sectional area size  $a_G$  and the chosen reference size  $a_m$ . The reference size was obtained by a standard optical diffraction instrument, which was used as a black box. It is not the purpose of this paper to discuss discrepancies between the size estimates obtained by the different measurement methods in detail. However, some remarks can be made to indicate that the results are within reasonable limits. The results are visualized in Fig. 10. For the sand and quartz particles the values of  $a_0$  mean that the acoustic size  $a_G$  is 20%–40% smaller than the optical diffraction size  $a_m$ . For the lead-glass beads, the acoustic size  $a_G$  is systematically somewhat lower, up to 15%, than the optical diffraction size estimate. These results are not unreasonable or unexpected. For the spherical lead-glass beads one expects the best agreement, since the optical diffraction instrument is calibrated for spherical particles, as are all standard particle sizing instruments. For the irregularly shaped sediment particles, the optical diffraction instrument will measure some effective size. Here it is relevant to note that Syvitski *et al.* have found that for a range of sand sediment samples, the size estimates obtained by an electrozone particle sizer were 17%–29% less than those obtained by an optical diffraction instrument.<sup>33</sup> The electrozone instrument

should provide an equal volume size estimate. From the present acoustic attenuation spectra, the equal volume radius can be derived from Eq. (9) as  $a_G/b_0^{1/3}$ , and using Eq. (8) to obtain  $a_G$ . The resulting values are 22%–49% less than the optical diffraction sizes for the sand and quartz particles. Therefore the difference between the present acoustic and optical diffraction size estimates is qualitatively consistent with the finding of Syvitski *et al.*

It is emphasized that a reference size is not required to determine the acoustic size  $a_G$  from a measured attenuation spectrum. Instead of taking some measured size estimate for  $a_m$ , one can take any (reasonable) initial guess and then determine  $a_0$  by the fitting procedure to obtain  $a_G$ . The values of  $b_0$  do not therefore depend upon  $a_m$  and the departure from the expected value of unity (of  $b_0$ ) for the lead-glass beads, discussed in the previous section, cannot be attributed to errors in the optical diffraction sizes. Thus  $a_0$  is a scaling parameter with no intrinsic physical meaning with respect to particle shape.

## C. Comparison with Flammer's data

In a previous study by Sheng and Hay, the measurements made by Flammer of attenuation in aqueous suspensions of sand in the frequency range of 2.5–25 MHz were compared to spherical scatterer theory.<sup>34,18</sup> The result of this comparison is shown in the left half of Fig. 13. It can be seen that as in the present investigation, the measured attenuation is greater than that predicted by rigid sphere theory and that there is also a slight shift to higher values of  $ka$  of the position of the main peak. These effects are also larger for the smaller sizes. The size estimates used for the  $ka$  scale were the midpoints  $d_s$  of the sieve intervals, so the measured radius  $a_m$ , as used in the above formal description, is equal to

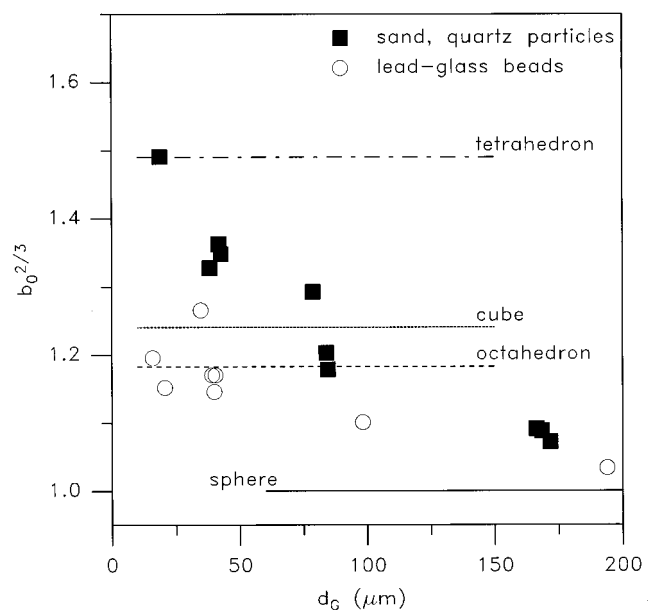


FIG. 12. The values of the parameter  $b_0^{2/3}$ , which correspond to the acoustically determined projected area relative to that of an equal volume sphere [cf. Eq. (9)], are summarized here as a function of the acoustically determined average size  $d_G$ . They are compared with the corresponding values for some simple polyhedral shapes, as further explained in the text.

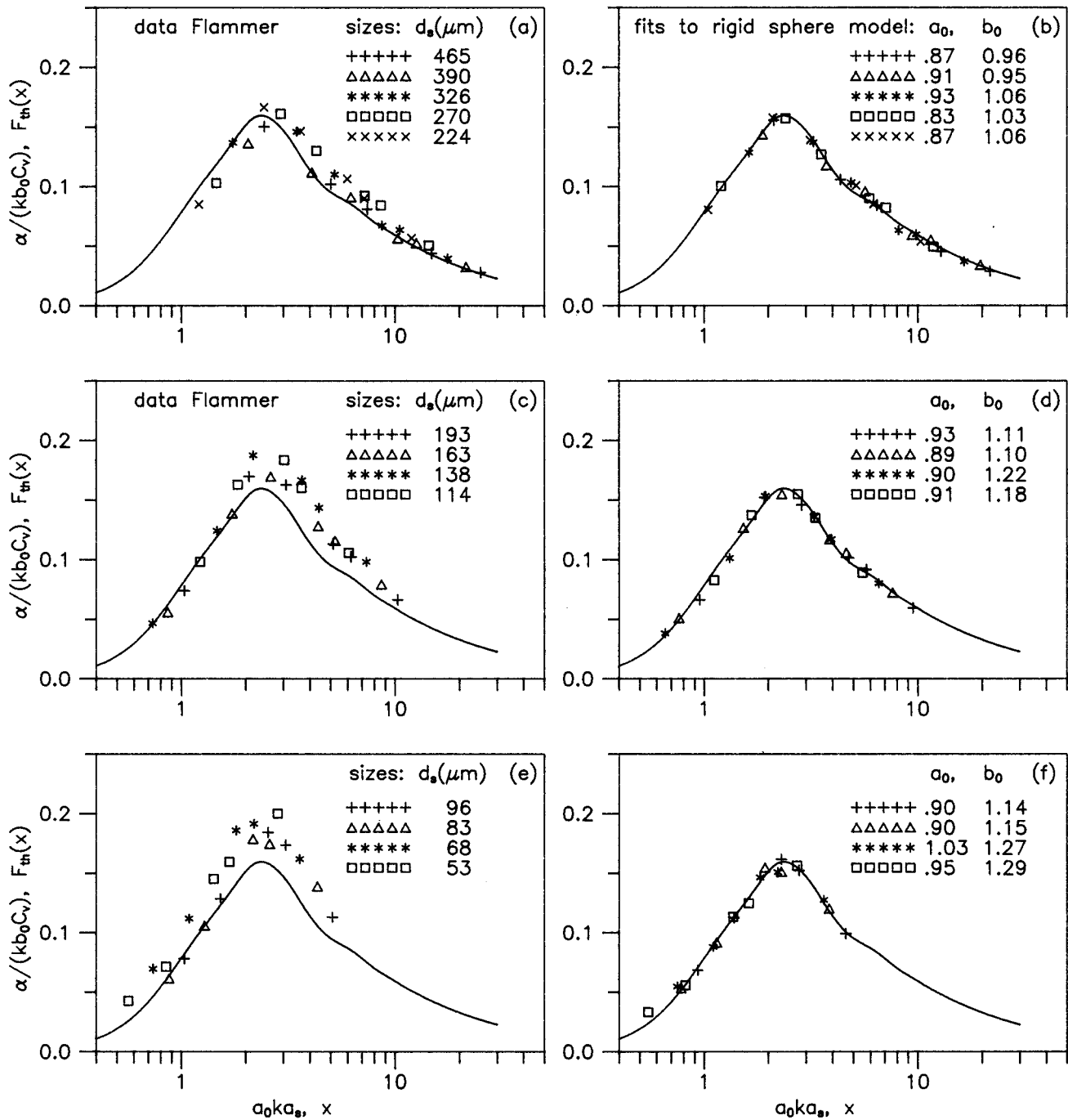


FIG. 13. Experimental data obtained by Flammer on 13 sieve size fractions made up from Missouri River and blasting sand (Ref. 18, Fig. 3, p. A16), compared with the theoretical model for a rigid movable quartz sphere. The data are presented in the same way as in Figs. 7–9 for the present study, with the exception that the average sieve size is used to normalize the acoustic wave number. Note that the average sieve diameters  $d_s$  are given with the as-measured spectra in the left half of the figure, and the parameter values  $a_0$  and  $b_0$  with the fitted measurements in the right half of the figure.

$d_s/2$  in the present case. The results of the two-parameter model analysis are given in the right half of Fig. 13, showing that also for these earlier measurements much better fits to the spherical scatterer theory are obtained, although there is quite a lot of scatter in Flammer's data and the spectra consist of a small number of points (maximum 6). It is consistent with the above remarks that the scaling parameters for Flammer's data show the same trends as those for the present study (see Fig. 14).

On the basis of Flammer's measurements, Sheng and Hay proposed that a modified version of Johnson's high-pass model could be used to represent the scattering cross section of natural sand particles,<sup>35</sup> in order to represent the higher measured attenuation compared to the computed values for a rigid sphere. This formulation has been used by a number of investigators to compute the scattering attenuation when inverting backscatter profiles to obtain profiles of suspended sand concentration.<sup>14–16,26</sup> However, in view of the present

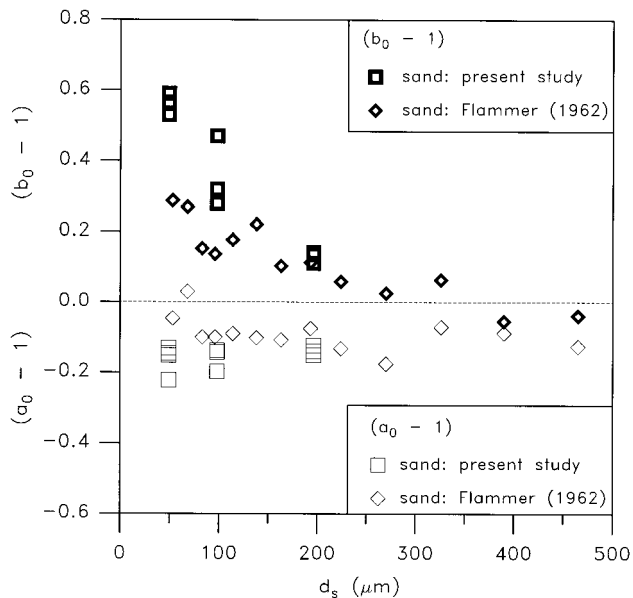


FIG. 14. Comparison of the two scaling parameters for Flammer's data (Fig. 13), with those for the sand sieve size fractions of the present study. Note that also for the latter data, the value of  $a_0$  given is related to the average sieve size, i.e.,  $a_0 = d_G/d_s$  [see Eq. (8)].

results, it is clear that the rigid sphere model can provide a very good fit to the data if the effects of irregular shape are taken into account. This result is appealing because the two-parameter spherical scatterer model attempts to include the relevant physics, whereas the high-pass model is purely *ad hoc*.

#### D. Viscous and thermal absorption

Thus far the measured attenuation has been attributed to scattering alone. There is also the possibility that viscous and thermal absorption may have contributed to the measurements. This possibility is briefly considered here.

Thermal absorption by natural sediment particles has been considered elsewhere.<sup>36</sup> It was found that viscous absorption was more important, in the long-wavelength region at least. It can also be argued that thermal losses remain small at shorter wavelengths. This argument is based on the theoretical and experimental work of Allegra and Hawley.<sup>37</sup> They have shown that the thermal losses peak at a value of the ratio of the particle radius to the thermal boundary layer thickness of the order of one. This ratio is much larger than one for all particles of the present study.

Viscous absorption is expected to be important mainly at long wavelengths, as first demonstrated by Urick.<sup>38</sup> An estimate of the contribution of viscous attenuation to the measured attenuation can also be made for medium and high frequencies, using the spherical scatterer theory.<sup>39,40</sup> The results of such calculations made for lead-glass spheres of the different average sizes of the present study can be summarized as follows. The contribution of the viscous attenuation for values of  $ka$  between 1 and 10 around the position of the maximum in the spectra of  $\alpha/(kb_0C_v)$  (cf. Fig. 6), is about 5% of the attenuation due to scattering alone for the smallest lead-glass particles ( $d_{50} = 17 \mu\text{m}$ , see Table III) and de-

creases with increasing particle size to about 1.2% for the largest size (i.e.,  $d_{50} = 196 \mu\text{m}$ ). Thus if the viscous attenuation were to be included in the theoretical model used for the two-parameter model analysis, the resulting values of  $b_0$  would be lower by maximum 5% for the smallest (lead-glass bead) size.

The above-mentioned results for lead-glass beads also provide an estimate of the importance of viscous absorption in the experiments with sand and quartz particles, as the grain densities of these materials are not markedly different from that of lead-glass. Thus it is estimated that for the sand and quartz particles, the maximum viscous attenuation would be 3% for the quartz particles and this would lead to a correspondingly lower value of  $b_0$ . This estimate is rather crude, however, as one would expect the viscous absorption to depend on the total surface area of the particles, and that this would be significantly larger for irregular particles than for spheres of a given equivalent size. Therefore it was felt necessary to test the importance of viscosity experimentally. This was done by measuring the attenuation spectrum for a 45–53- $\mu\text{m}$ -diam sieve size fraction of sand particles as well as of lead-glass beads at three different temperatures: 10, 20, and 30 °C. The viscosity of water changes by 50% over this temperature range, and one would expect to observe a change in the attenuation spectrum if viscous absorption were important. However, no significant changes were observed above  $x = 1$ , as is indicated by the values of  $a_0$  and  $b_0$  obtained from these measurements (see Tables II and III).

In view of the above discussion, it is concluded that, by neglecting the viscous attenuation, the values of  $b_0$  have been overestimated a little, however, by a maximum 5% only. It may also be concluded from the calculations of the viscous attenuation, that for particle sizes of about 20  $\mu\text{m}$  and smaller it is necessary to include viscous effects in an accurate analysis of attenuation spectra at these frequencies.

#### IV. CONCLUSIONS

It has been shown that measurements of attenuation spectra in turbulent suspensions of irregular sand and silt-sized particles can be brought into agreement with rigid spherical scatterer theory, but only by invoking two different equivalent sizes. The use of two sizes is appealing on physical grounds. One size is the diameter of a circle with equal projected (i.e., geometric) area, which is the natural scale for the total scattering cross section in the high-frequency limit. This size is used to scale the acoustic wave number, the abscissa of the attenuation spectrum. The second equivalent size is the diameter of the equal volume sphere, which is the natural scale for converting the volume concentration of particles to their number density. This size is used to scale the magnitude of the attenuation, which is the ordinate of the attenuation spectrum. In actual fact, the rescaling factor for the ordinate is a combination of the two equivalent sizes, since the projected area of the particle also affects the magnitude of the attenuation. Because the choice was made to emphasize the region in the vicinity of  $ka = 2$ , the vertical scaling factor ( $1/b_0$ ) appears here as the ratio of the actual particle volume to the volume based upon the size of the equal area sphere.

The two-parameter spherical scatterer model provides good agreement not only with the attenuation measurements for suspensions of natural sand and ground quartz presented here, but also with the much earlier measurements in sand suspensions made by Flammer.<sup>18</sup> The attenuation appears to be enhanced, i.e.,  $b_0 > 1$ , in all cases studied. The estimates of  $b_0$  are larger than expected for the smaller-sized lead-glass beads, although still less than the values for irregularly shaped particles in the same size range. It is suggested that inhomogeneities in the composition of the smaller beads (most probably interior defects, inferred from low grain densities and directly observed by scanning electron microscope) are responsible for the observed extra scattering. Unfortunately, therefore, the results obtained for the nominally spherical lead-glass beads do not provide direct support for the above interpretation in terms of a shape effect only, nor do they contradict it. However, direct support for the existence and approximately correct magnitude of the shape effect as found in the present study, is provided by numerical calculations of the orientation average total scattering cross section for a number of irregularly shaped bodies, of which some preliminary results have been published<sup>41</sup> and a comparison with experimental data is underway.<sup>42</sup>

The present results bring into focus the role of grain shape in the propagation of sound through suspensions of moderately irregular particles, natural and otherwise. The effects of grain shape on quantitative estimates of the concentration of suspended particles in marine environments using acoustic remote sensing techniques have largely been ignored. Present results are cautionary, suggesting that shape effects are potentially important, especially in the fine sand and silt-sized range, at the MHz frequencies commonly used in acoustic backscatter systems. This might be seen as further complicating the problem of inverting acoustic backscatter measurements to obtain particle concentrations. The more positive view is that the relatively simple theory for a spherical scatterer provides such good agreement with the measurements. This good agreement implies that spherical scatterer theory can be used in inversion algorithms, provided account is taken of the need for the two equivalent sizes.

## ACKNOWLEDGMENTS

The authors thank Nico Berkhoudt, Koos Wenneker, and Wim Taal of Delft Hydraulics for their efforts in realizing the acoustic measurements and providing technical support. The SEM micrographs were made at Memorial University of Newfoundland with the assistance of C. Emerson. The authors acknowledge support for their collaboration by a NATO Collaborative Research Grant (No. 890551). This research was further supported by grants to A.H. from the Natural Sciences and Engineering Research Council of Canada and to A.S. by grants from the Department of Hydro-Instrumentation of the Dutch Ministry of Transport, Public Works and Water Management and from Delft Hydraulics.

<sup>1</sup>R. A. Young, J. T. Merrill, T. L. Clarke, and J. R. Proni, "Acoustic profiling of suspended sediments in the marine bottom boundary layer," *Geophys. Res. Lett.* **9**, 175–178 (1982).

<sup>2</sup>A. E. Hay, "On the remote acoustic detection of suspended sediment at

long wavelengths," *J. Geophys. Res.* **88**, 7525–7542 (1983).

<sup>3</sup>F. R. Hess and K. W. Bedford, "Acoustic backscatter system (ABSS): the instrument and some preliminary results," *Mar. Geol.* **66**, 357–380 (1985).

<sup>4</sup>D. M. Hanes and D. A. Huntley, "Continuous measurements of suspended sand concentration in a wave-dominated nearshore environment," *Cont. Shelf Res.* **6**, 585–596 (1986).

<sup>5</sup>A. S. Schaafsma and W. J. G. J. der Kinderen, "Ultrasonic instruments for the continuous measurement of suspended sand transport," in *Proceedings of the IAHR Symposium on Measuring Techniques in Hydraulic Research*, edited by A. C. E. Wessels (Balkema, Rotterdam, 1986), pp. 125–136.

<sup>6</sup>A. S. Schaafsma and A. J. Wolthuis, "Frequency dependence of the interaction of ultrasound with suspended sediment particles," in *Progress in Underwater Acoustics*, edited by H. M. Merklinger (Plenum, New York, 1986), pp. 153–160.

<sup>7</sup>D. V. Holliday, "Acoustic determination of suspended particle size spectra," *Coastal Sediments '87*, 260–271 (1987).

<sup>8</sup>K. R. Dyer and R. L. Soulsby, "Sand transport on the continental shelf," *Annu. Rev. Fluid Mech.* **20**, 295–324 (1988).

<sup>9</sup>D. M. Hanes, C. E. Vincent, D. A. Huntley, and T. L. Clarke, "Acoustic measurements of suspended sand concentration in the C<sup>2</sup>S<sup>2</sup> experiment at Stanhope Lane, Prince Edward Island," *Mar. Geol.* **81**, 185–186 (1988).

<sup>10</sup>J. F. Lynch and Y. C. Agrawal, "A model-dependent method for inverting vertical profiles of scattering to obtain particle size spectra in boundary layers," *Mar. Geol.* **99**, 387–401 (1991).

<sup>11</sup>J. F. Lynch, T. F. Gross, B. H. Brumley, and R. A. Filyo, "Sediment concentration profiling in HEBBLE using a 1-MHz acoustic backscatter system," *Mar. Geol.* **99**, 361–385 (1991).

<sup>12</sup>C. E. Vincent and M. O. Green, "Field measurements of the suspended sand concentration profiles and fluxes and of the resuspension coefficient  $\gamma_0$  over a rippled bed," *J. Geophys. Res.* **95**, 11591–11601 (1990).

<sup>13</sup>C. E. Vincent, D. M. Hanes, and A. J. Bowen, "Acoustic measurements of suspended sand on the shoreface and the control of concentration by bed roughness," *Mar. Geol.* **96**, 1–18 (1991).

<sup>14</sup>P. D. Thorne, C. E. Vincent, P. J. Hardcastle, S. Rehman, and N. Pearson, "Measuring suspended sediment concentrations using acoustic backscatter devices," *Mar. Geol.* **98**, 7–16 (1991).

<sup>15</sup>P. D. Thorne, P. J. Hardcastle, and R. L. Soulsby, "Analysis of acoustic measurements of suspended sediments," *J. Geophys. Res.* **98**, 899–910 (1993).

<sup>16</sup>A. E. Hay and J. Sheng, "Vertical profiles of suspended sand concentration and size from multifrequency acoustic backscatter," *J. Geophys. Res.* **97**, 15661–15677 (1992).

<sup>17</sup>W. G. Bos, "A comparison of two Doppler current profilers," *IEEE J. Ocean Eng.* **16**, 374–381 (1991).

<sup>18</sup>G. H. Flammer, "Ultrasonic measurement of suspended sediment," *Geological Survey Bulletin No. 1141-A* (US Government Printing Office, Washington, DC, 1962).

<sup>19</sup>V. K. Varadan, V. N. Bringi, V. V. Varadan, and Y. Ma, "Coherent attenuation of acoustic waves by pair-correlated random distributions of scatterers with uniform and Gaussian distributions," *J. Acoust. Soc. Am.* **73**, 1941–1947 (1983).

<sup>20</sup>A. S. Schaafsma, "Acoustic measurement of concentration and size of sediment particle suspensions," in *Proceedings Ultrasonics International '89* (Butterworth, Washington, DC, 1989), pp. 388–393.

<sup>21</sup>A. E. Hay and A. S. Schaafsma, "Resonance scattering in suspensions," *J. Acoust. Soc. Am.* **85**, 1124–1138 (1989).

<sup>22</sup>A. S. Schaafsma, "Empirical 2-parameter model for acoustic attenuation spectra—Development of silt measuring methods," *Delft Hydraulics Progress Report B260*, 1992, 25 pp.

<sup>23</sup>A. S. Schaafsma, "Acoustic attenuation spectroscopy of suspended sediments," in *2nd European Conference on Underwater Acoustics*, edited by L. Björnó (European Commission, Luxembourg, 1994), Vol. 2, pp. 863–868.

<sup>24</sup>A. S. Schaafsma, "Particles of irregular shape, scattering and multicomponent mixtures—Development of silt measuring methods," *Delft Hydraulics Progress Report F37*, 1991, 47 pp.

<sup>25</sup>A. E. Hay, "Sound scattering from a particle-laden turbulent jet," *J. Acoust. Soc. Am.* **90**, 2055–2074 (1991).

<sup>26</sup>A. M. Crawford and A. E. Hay, "Determining suspended sand size and concentration from multifrequency acoustic backscatter," *J. Acoust. Soc. Am.* **94**, 3312–3324 (1993).

<sup>27</sup>C. He and A. E. Hay, "Broadband measurements of the acoustic back-

- scatter cross section of sand particles in suspension," J. Acoust. Soc. Am. **94**, 2247–2254 (1993).
- <sup>28</sup>F. H. Fisher and V. P. Simmons, "Sound absorption in sea water," J. Acoust. Soc. Am. **62**, 558–562 (1977).
- <sup>29</sup>J. M. M. Pinkerton, "A pulse method for the measurement of ultrasonic absorption in liquids: Results for water," Nature (London) **160**, 128–129 (1947).
- <sup>30</sup>R. E. Carver, *Procedures in Sedimentary Petrology* (Wiley, New York, 1971).
- <sup>31</sup>H. C. van de Hulst, *Light Scattering by Small Particles* (Dover, New York, 1981), p. 110.
- <sup>32</sup>R. Hickling, "Analysis of echoes from a hollow metallic sphere in water," J. Acoust. Soc. Am. **36**, 1124–1137 (1964).
- <sup>33</sup>J. P. M. Syvitski, K. W. G. Leblanc, and K. W. Asprey, in *Principles, Methods, and Application of Particle Size Analysis*, edited by James P. M. Syvitski (Cambridge U.P., Cambridge, England, 1991), Chap. 13.
- <sup>34</sup>J. Sheng and A. E. Hay, "An examination of the spherical scatterer approximation in aqueous suspensions of sand," J. Acoust. Soc. Am. **83**, 598–610 (1988).
- <sup>35</sup>R. K. Johnson, "Sound scattering from a fluid sphere revisited," J. Acoust. Soc. Am. **61**, 375–377 (1977).
- <sup>36</sup>A. E. Hay and R. W. Burling, "On sound scattering and attenuation in suspensions, with marine applications," J. Acoust. Soc. Am. **72**, 950–959 (1982).
- <sup>37</sup>J. R. Allegra and S. A. Hawley, "Attenuation of sound in suspensions and emulsions: theory and experiments," J. Acoust. Soc. Am. **51**, 1545–1564 (1972).
- <sup>38</sup>R. J. Urlick, "The absorption of sound in suspensions of irregular particles," J. Acoust. Soc. Am. **20**, 283–289 (1948).
- <sup>39</sup>A. E. Hay and D. G. Mercer, "On the theory of sound scattering and viscous absorption in aqueous suspensions at medium and short wavelengths," J. Acoust. Soc. Am. **78**, 1761–1771 (1985).
- <sup>40</sup>A. E. Hay and D. G. Mercer, "A note on the viscous attenuation of sound in suspensions," J. Acoust. Soc. Am. **85**, 2215–2216 (1989).
- <sup>41</sup>T. Mazoyer and D. Guyomar, "Sediment scattering modelling by boundary elements," in *2nd European Conference on Underwater Acoustics*, edited by L. Bjørnø (European Commission, Luxembourg, 1994), Vol. 2, pp. 911–916.
- <sup>42</sup>A. S. Schaafsma, A. M. Lafort, T. Mazoyer, and D. Guyomar, "Characterization of suspended sediment by acoustic techniques, Part I: Theoretical and experimental validation of attenuation spectroscopy," Acta Acust. (to be published).